Grouping of Clouds in a Numerical Cumulus Convection Model

A. van Delden and J. Oerlemans
Institute for Meteorology and Oceanography, University of Utrecht Princetonplein 5, Utrecht, The Netherlands

(Manuscript received 09.11.1981, in revised form 16.04.1982)

Abstract: Simulations with a two-dimensional numerical model of cumulus convection with random forcing are presented. The domain size is 4 by 60 km, with a grid distance of 200 m. We have carried out a number of 5 h real time simulations. The results show that, if convection is deep enough, cumulus clouds tend to occur in groups. A typical cloud size is 3 km, whereas cloud groups have a diameter of about 15 km. Downdraughts play an important role in producing these groups.

For shallow convection this grouping or clumping of clouds does not take place, although the flow in this case is also strongly organized (formation of stratocumulus). The factors responsible for organizing the flow are examined.

Zusammenfassung: Gruppierung von Wolken in einem numerischen Modell der Cumulus Konvektion.

Die Arbeit zeigt Simulationsergebnisse mit einem zweidimensionalen numerischen Modell der Cumulus Konvektion mit einer Zufalls-Antriebsfunktion. Das Integrationsgebiet besitzt eine Größe von 4 km (Höhe) X 60 km mit einem Gitterabstand von 200 m. Eine Reihe von Simulationen über 5 h (Realzeit) wurden durchgeführt. Die Ergebnisse zeigen, daß bei genügend tiefer Konvektion die Cumuluswolken dazu neigen sich in Gruppen zu ordnen. Eine typische Wolkengröße ist 3 km, die Wolkengruppen haben dabei einen Durchmesser von etwa 15 km. Bei der Entwicklung dieser Gruppen spielen die Abwärtsbewegungen eine bedeutende Rolle.

Bei flacher Konvektion ergibt sich keine derartige Gruppenbildung, obwohl die Strömung in diesem Falle auch stark organisiert erscheint (Bildung von Stratocumulus). Die für die geordnete Strömung verantwortlichen Faktoren werden untersucht.

Résumé: Groupement de nuages dans un modèle numérique de convection cumuliforme

On présente des simulations numériques à deux dimensions de la convection cumuliforme, avec maille de 200 m. On a exécuté une série de simulations sur 5 heures (en temps réel). Les résultats montrent que, si la convection est suffisamment profonde, les cumulus ont tendance à s'organiser en groupes. Une dimension typique de nuage est 3 km, tandis que les groupes de nuages ont un diamètre d'environ 15 km. Les mouvements descendants jouent un rôle important dans la formation de ces groupes.

Si la convection est peu profonde, ce groupement de nuages ne se produit pas, bien que l'écoulement soit également dans ce cas fortement organisé (formation de stratocumulus). On étudie les facteurs responsables de cette organisation de l'écoulement.

1 Introduction

One of the features of cumulus clouds that has rarely been studied theoretically or numerically is their tendency to occur in groups or clumps, especially when convection has been going on for more than a few hours. RANDALL and HUFFMAN (1980) define a clump as a group of cumulus clouds whose members are much more closely spaced than the average spacing over the population, and which main-

0303-4186/82/02 0239-14 $ 02.00/0

tains its identity over many cloud lifetimes. Such clumps can easily be observed on high-resolution satellite pictures, and occur frequently. In most cases the inhomogeinity of the surface conditions or the presence of strong wind shear are assumed to control clumping. However, in some other cases such causes seem to be absent (for example, summer conditions over Florida frequently come in this class).

On a typical summer day over Florida, clumps almost always develop around midmorning. During the first two hours of cumulus convection the clouds are relatively small and spaced more or less uniformly, whereas in the afternoon clumps form (PLANK, 1969). The clumps seem to have nothing to do with a particular synoptic situation, neither is there any correlation with ground characteristics. There must therefore be a cloud-scale dynamical mechanism that controls the formation of clumps and their maintenance through time. In view of this, it is worthwhile to investigate whether cloud models can produce clumping of clouds when forced in a random manner. Analysis of model results can then shed some light on the mechanisms that organize cumulus clouds.

HILL (1974) integrated a two-dimensional cloud model with random heating from below for several hours, i.e. through the initiation, growth and fully developed stages of cumulus clouds. He could thus examine the factors controlling the size, spacing and merging of cumulus clouds. He found that during the initial stage the dominant factor governing the size and spacing is the subcloud circulation. During the growth stage the spacing is governed mainly by the size of competing cloud circulations. In the fully-developed stage many factors play a role, notably moisture anomalies left behind by the decay of the big clouds, favouring the formation of new clouds at the same location. However, the model domain (16 km in the horizontal) was too small to simulate more than one multicell cloud circulation in the fully developed stage.

In this study we go further along this line. At the cost of less sophisticated cloud physics (no ice) and more simple dynamics (anelastic equations) we expanded the model domain to 60 km in the horizontal. With a 4 km height of the model atmosphere and a grid spacing of 200 m, this yields a considerable amount of grid points. The model we developed is very similar to that of MURRAY (1970), we therefore describe it only briefly in the Appendix.

With this model a number of integrations were carried out, in most cases 5 hr real time simulations. In spite of its 'two-dimensionality' and the lack of varying surface conditions, the model appears to create grouping of cumulus clouds under completely random forcing. In the following we present an overview of the results and discuss the mechanisms responsible for the clumping of the model clouds.

2 Description of the model

Here we only give a brief summary of the cloud model. Equations, a list of symbols, and a discussion on some technical aspects are given in the Appendix.

The model is formulated for a two-dimensional domain, which permits the use of a streamfunction. The domain width and height are 60 km and 4 km respectively, and the grid interval is 200 m. The dynamical state is computed with a vorticity equation in which the buoyancy is the driving force. The Boussinesq approximation is used, and the air is assumed to be incompressible.

The calculation of the variables temperature, mixing ratio of water vapour and mixing ratio of liquid water is done in a Lagrangian manner. This involves the computation of a backward trajectory for each gridpoint, along which thermodynamics are then applied (see Appendix for more detail).

The model does not consider precipitation. All liquid water is carried with the air and is always available for evaporation. There is no formation of ice.

Eddy diffusion of momentum, heat, water vapour and liquid water is parameterized using the K-theory where all diffusion coefficients are equal and constant (25 m^2/s). We found that this value gives the best

agreement between observed and model clouds. TAG et al. (1979), in studying the effects of different diffusion coefficients, obtained a similar value as the best.

No motion is allowed at any boundary and all values of T, r_v and r_l are held constant at their initial values, except at the bottom boundary where the forcing is applied. With these boundary conditions the clouds do not 'stick' to the lateral and top boundaries.

3 Forcing

An atmospheric sounding made at Cabauw (The Netherlands) at 8:33 GMT on June 23, 1981, a day on which small to intermediate size cumulus clouds formed at midmorning, obviously as a result of solar heating of the ground, and dissipated at the end of the afternoon, was used as initial condition. The sounding was made at about the time the first small cumulus clouds appeared.

In order to initiate and maintain convection perturbations are necessary. We organized this in the following way.

The changes of temperature and water vapour of a layer of constant density ρ can be expressed as

$$\frac{\partial T}{\partial t} = \frac{\Phi_s}{\rho c D_z} \quad \text{and} \quad \frac{\partial r_v}{\partial t} = \frac{\Phi_L}{L \rho D_z} \tag{1}$$

where Φ_s and Φ_L are respectively the fluxes of thermal enthalpy and latent enthalpy, $c(=c_p + c_{pv} r_v + c_w r_l)$ is the weigthed specific heat capacity of the mixture of air, water vapour and liquid water and D_z is the thickness of the layer to which the enthalpy is added.

The definition of the Bowen ratio (B_R) is $B_R = \Phi_s/\Phi_L$ (2)

(1) and (2) can be combined to yield

$$\frac{\partial r_v}{\partial t} = \frac{C}{L B_R} \frac{\partial T}{\partial t}. \tag{3}$$

If we prescribe $\partial T/\partial t$ for the lowest layer and specify a Bowen ratio, $\partial r_v/\partial t$ for the same layer can be calculated from (3). $\partial T/\partial t$ is prescribed in the form of perturbations at 200 m and at the "ground". Because the boundary conditions do not permit any motion at the ground, only the perturbations at 200 m initiate convection.

The temperature perturbations are prescribed continuously in a random manner. If C_T is the probability, per timestep (Δt) and per gridpoint, that there will be a perturbation and P_T is the magnitude of the temperature perturbation, then we can write,

$$\frac{\partial T}{\partial t} = \frac{C_T P_T}{\Delta t} \tag{4}$$

If we substitute this in (3) we get

$$\frac{\partial r_v}{\partial t} = \frac{c C_T P_T}{B_R L \Delta t}. \tag{5}$$

The change in mixing ratio of watervapour r_v, as a result of evaporation from the ground, is prescribed at 0 and 200 m according to (5). For the temperature perturbations use is made of a random generator which generates random numbers between 0 and 1. At any gridpoint temperature is increased by P_T °C if the random number is lower than C_T. The value of P_T was chosen to be 1 °C, except for one of the runs when it was fixed at 0.75 °C. These values correspond to observed temperature excesses of thermals at a height of about 200 m (WARNER and TELFORD, 1967).

Table I Survey of the runs

Run	Running time (real time in hrs)	Domain size X (km)	Z	Forcing C_T	P_T(K)	
1	5	60	4	1/360	1.0	
2	5	60	4	1/360	1.0	different random number set
3	5	60	4	1/360	1.0	
4	5	60	4	1/360	1.0	identical to run 3 except $C_T = 0$ after 2.5 h
5	5	60	4	1/360	1.0	identical to run 2 except $C_T = 0$ for $34 < X < 40$ km
6	5	60	2.2	1/540	0.75	
7	8	60	2.2	1/540	0.75	continuation of run 6 for 3 h without forcing
7*	5	60	2.2	1/540	0.75	identical to run 6 except $C_T = 0$ after 2.5 h

Table I gives a survey of the runs. We did seven runs of 5 hours real time, with a timestep of 10 s: five runs with the top boundary at 4 km and with different forcing conditions, and two runs with the top boundary at 2.2 km, approximately corresponding to the location of inversion at initial time. The forcing in the first five runs was always 1 °C per hour, per grid point at 0 and 200 m (C_T = 1/360, P_T = 1 °C). The first three runs only differ in the random number set which was generated to determine the perturbations. The fourth run is identical to the third except that the forcing was stopped after 2.5 hours. The fifth run is identical to the second except that tehre was no forcing between x = 34 km and x = 40 km. In the sixth run the forcing was halved (C_T = 1/540, P_T = 0.75 C). This was more realistic for the day the atmospheric sounding was made. However, it should be stressed that it was not our aim to simulate the evolution of cumulus convection on that particular day, but rather to examine the factors controlling the interaction between cumulus clouds. Run 7 is a continuation of run 6 for three hours, without forcing. The Bowen ratio was fixed at 0.5 for all runs.

4 Results

In Figures 1 and 2 the evolution of the cumulus cloud patterns are shown in running-time diagrams. In these pictures, the effective cloud cross-section, as viewed from 'space', is shown. So whenever liquid water is present in the column, at any height, the gridpoint is cloudy (black in the Figures). Most striking in the first five runs (strong forcing, Figures 1, a–e) is that after about two hours of convection the more or less uniform spacing of the clouds changes into a group structure with a typical scale of 15 to 30 km. For the last three hours of simulation, runs 1, 2 and 3 (Figures 1a, b, c), which only differ in the random number set used to determine the perturbations, show respectively two, one and two permanent clumps. Run 4 (Figure 1d), in which the forcing was turned off after 2.5 hours, shows a remarkable similarity to the pattern produced by run 3 (Figure 1c), which is identical except that the forcing is continued. This similarity can also be seen in Figure 3 which shows the evolution in time of the kinetic energy KE (defined as the sum of $1/2\ (u^2 + w^2)$ over all gridpoints devided by the total number of gridpoints) for these runs. Evidently the model has a very retentive memory; in other words the forcing does not dominate the dynamics of the circulation very much after 2.5 hours. For 1.5 hours after the heating was turned off the two curves keep pace, before they ultimately diverge.

In run 5 no forcing is applied between x = 34 km and x = 40 km. As expected no clouds form over the 'lake' and clouds which try to cross it soon dissipate.

Although the results of run 6 (Figure 2) seem similar to the results of the other runs in that the cloud cover becomes organized, this organization is significantly different in character in the later stage of

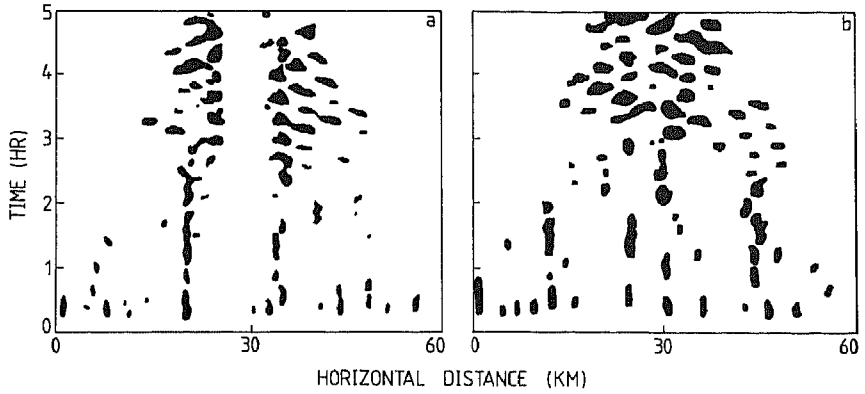

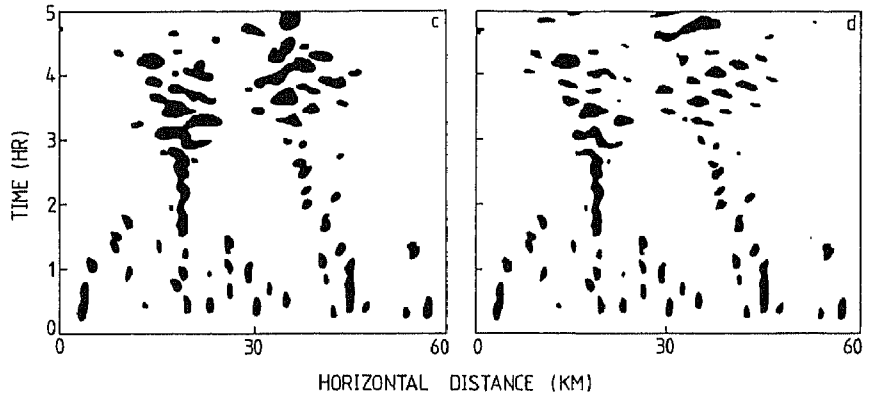

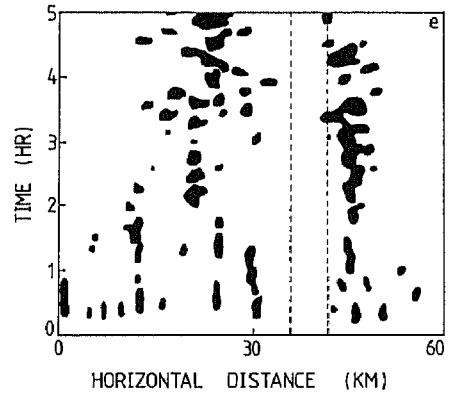

- **Fig. 1** Cloud cover as a function of time and horizontal distance for five model runs. The runs displayed in a, b and c only differ with respect to the random number set used in the forcing. Results in panel d are obtained by switching off the forcing after 2.5 h. The last panel (e) shows a run in which the forcing was zero for 34 km $< X <$ 40 km. The results shown in this figure correspond to runs 1–5 in Table I.

- **Bild 1** Bewölkung als Funktion von Zeit und Horizontalkoordinate für fünf Modell-Läufe. Die Ergebnisse in a, b und c unterscheiden sich nur in Bezug auf den Satz der Zufallszahlen, die bei der Antriebsfunktion benutzt wurden. Bei d wurde der Antrieb nach 2,5 h abgestellt; bei e war der Antrieb Null für 34 km $< X <$ 40 km. Dies sind Ergebnisse der Rechenläufe 1 bis 5; sie sind in Tabelle I näher erläutert.

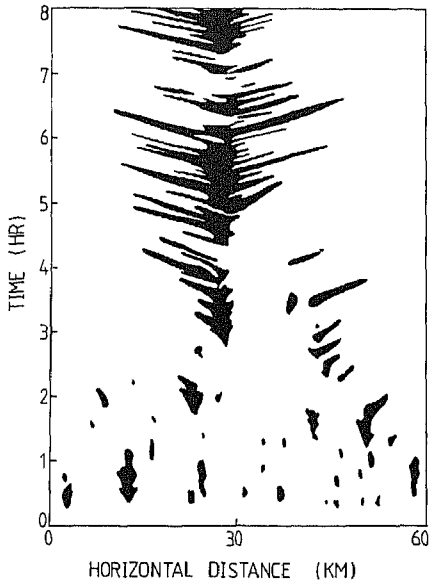

- Fig. 2 Cloud cover in a run with shallow convection (runs 6 and 7 in Table I). The heating is set to zero after 5 h.
- Bild 2 Bewölkung in einem Rechenlauf mit flacher Konvektion (Läufe 6 und 7 in Tabelle I). Die Erwärmung wurde nach 5 h auf Null gesetzt.

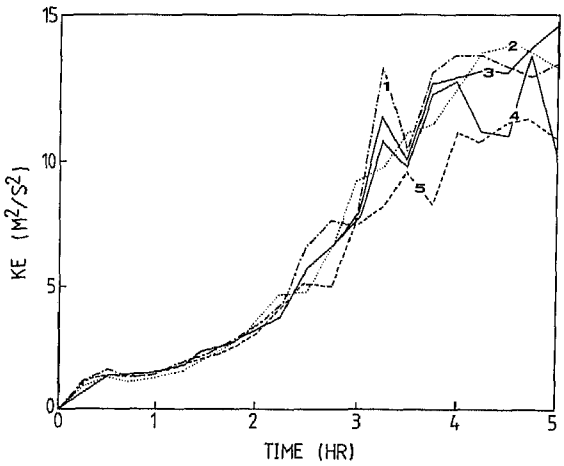

- Fig. 3 Kinetic energy as a function of time for the runs with strong convection. Labels refer to Table I.
- Bild 3 Kinetische Energie als Funktion der Zeit für die Rechenläufe mit starker Konvektion. Die Zahlen an den Kurven stellen die Zuordnung zu Tabelle I her.

convection. After about 2.5 hours there is one location (at x = 27 km) at which clouds persistently form. Smaller clouds break away from the mother cloud, which more resembles a stratocumulus layer, at this location and move to the left, and later also to the right, over distances of 3 to 20 km before the environment becomes too dry and they dissipate. The distances they travel become greater as time progresses, probably because preceding clouds leave behind moisture anomalies.

We shall now give a qualitative account of what happens in the first five runs and examine why, after a certain time, clumping occurs.

During the first one or two hours of convection small cumulus clouds with lifetimes of about 15 to 45 minutes develop. The updraughts, which are in general more intense in the subcloud layer, are much more pronounced than the downdraughts. The air descends gradually over a relatively large area

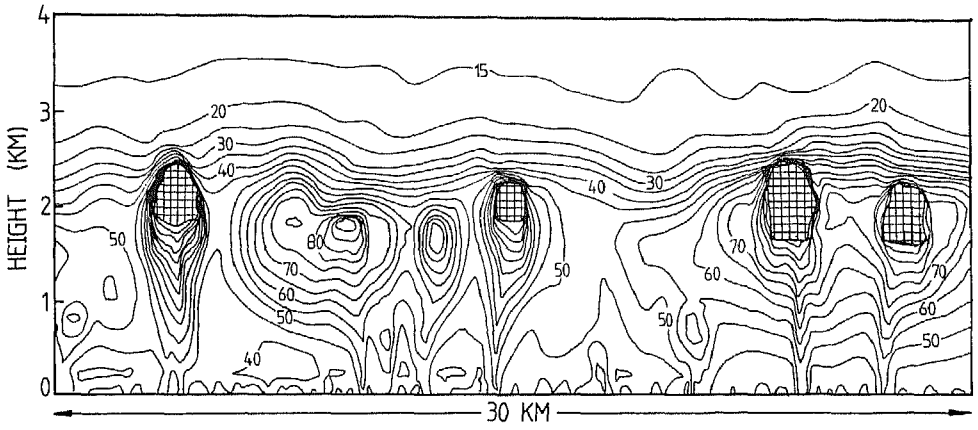

- **Fig. 4** Part of a typical moisture field in the initial stage of strong convection (run 5, t = 75 min). The quantity shown is relative humidity. Liquid water is indicated by hatching. The inversion that is present initially can be seen clearly in the moisture field.

- **Bild 4** Teil eines typischen Feldes der relativen Feuchte im Anfangsstadium starker Konvektion (Rechenlauf 5, $t = 75$ min). Das Vorhandensein von Flüssigwasser ist durch die Schraffur angedeutet. Die anfänglich vorhandene Inversion läßt sich deutlich im Feuchte-Feld erkennen.

on either side of the cloud. The inversion is gradually eroded. The average cloud base rises from 1500 m for the first clouds to 1800 m after 3 hours. Figure 4 shows a typical moisture field in the initial stage (t = 75 min).

The convection gradually becomes organized into a few cells which have grown at the expense of others. This organization is accompanied by an organization of the water vapour into dry and wet regions (this also happens in run 6 (shallow and weak convection)). In these last regions conditions become such that cumulus congestus clouds (size: 2.5–5 km in diameter and 1.5–2 km in depth) can form after about two hours. At this stage a new organizing mechanism begins to play a role, namely, the downdraughts associated with these big clouds. In the following we shall explain qualitatively what happens.

Because large amounts of latent heat are released at the cloud base (the maximum cloud water content is frequently more than 2 g/kg), and because of its inertia, the rising air can penetrate deep into the stable layer. Generally the top half of the cloud is therefore colder than its environment. This is in agreement with observations (TELFORD and WARNER, 1962).

The condensed water is evaporated again at the cloud edges. Thereby latent heat is created from sensible heat and hence the cloud edges become relatively cold. The air at an intermediate distance from the cloud is stable, because it has been warmed by subsidence of dry, stable air from aloft. This situation benefits the confinement of the downdraught to a small area around the edges. Figure 5 illustrates these findings. Apparently, the downdraughts are just as intense as the updraughts, which reach a maximum just below the cloud base. Sometimes the downdraughts are partly inside the cloud. Figure 6 shows the evolution of the maximum up- and downdraughts for runs 3, 4 and 6. Only when the inversion is not permitted to be eroded (run 6) do the downdraughts never acquire the same intensity as the updraughts. The clouds in this case are shallow (200–800 m in depth) and the water content never exceeds 0.8 g/kg. Therefore evaporation at the cloud edges is too small to produce significant temperature anomalies. Nevertheless, the cloud cover is strongly organized. Moisture accumulates below the inversion and there is a tendency to produce a stratocumulus deck. Moisture anomalies

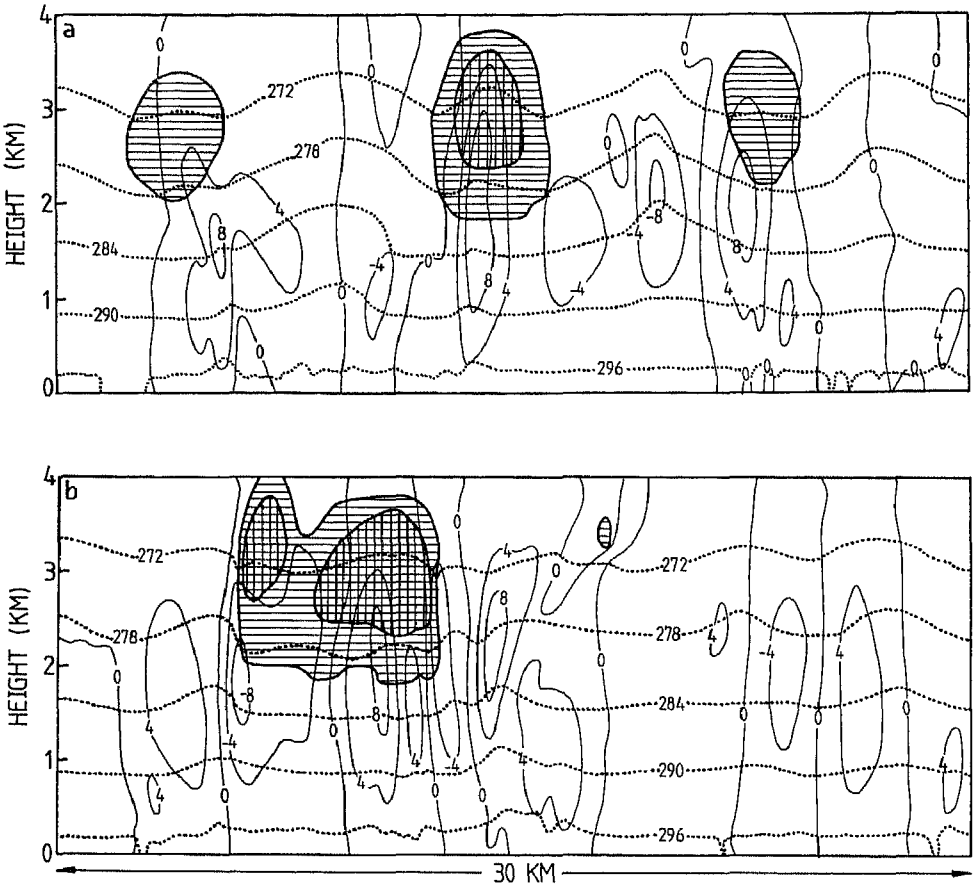

- **Fig. 5** Structure of strong convection in the model, in terms of the vertical motion field (solid lines, m/s) and virtual temperature (dotted lines, K). Liquid water is indicated by hatching; double hatching shows regions where the liquid water mixing ratio exceeds 0.75 g/kg. Panel b shows the situation in run 2 after 5 h, 15 min after that in panel a. The small cumulus cloud on the lefthand side in panel a develops into a cumulus congestus cloud in b. The latter creates strong downdraughts.

- **Bild 5** Modell-Struktur starker Konvektion dargestellt durch die Vertikalbewegung (ausgezogen, in m/s) und die virtuelle Temperatur (gepunktet, in K). Der Flüssigwassergehalt ist durch die Schraffur angedeutet; die doppelte Schraffur zeigt Gebiete, in denen der Flüssigwassergehalt 0,75 g/kg überschreitet. Teil b zeigt die Verhältnisse beim Rechenlauf 2 nach 5 h, Teil a gibt die Situation 15 min eher wieder. Die kleine Cumulus-Wolke links in Bild 5a entwickelt sich zu einem Cu con in 5 b, der starke Abwinde hervorruft.

break from the main cloud and drift away. A typical cross section of this situation is shown in Figure 7.

5 Discussion

The first thing to note from this study is that in a comparatively simple model of convection in a moist atmosphere, organization occurs. Apparently the processes necessary to cause grouping of clouds are present in a two-dimensional model (which does not mean that we expect completely sim-

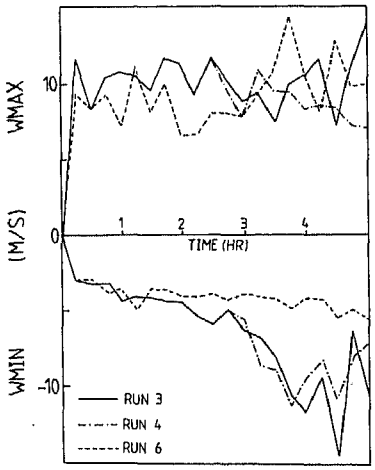

- **Fig. 6** Maximum up- and downdraughts in the model domain for runs 3, 4 and 6.

- **Bild 6** Maxima der Auf- und Abwinde im Modellgebiet bei den Rechenläufen 3, 4 und 6.

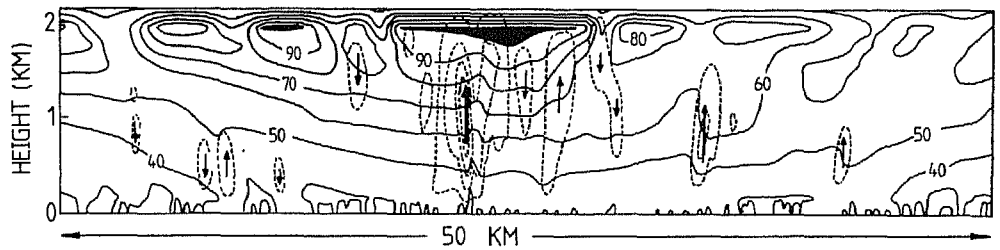

Fig. 7 Relative humidity (solid lines, %) and vertical motion (dashed lines, − 3, − 1, ... m/s) at t = 5 h for run 6. Black areas show the presence of liquid water.

Bild 7 Relative Feuchte (ausgezogen, in %) und Vertikalwind (gestrichelt, − 3, − 1, ... m/s) bei Rechenlauf 6 zur Zeit t = 5 h. Die schwarzen Gebiete zeigen das Vorhandensein von Flüssigwasser.

ilar results in three dimensions). Also gravity waves are not needed to generate organized patterns. Irrespective of the type of organization, it seems that the interaction between moisture field and dynamics is the decisive factor. According to our results, the nature of this interaction is different for weak (or shallow) and strong cumulus convection.

In the case of strong, sufficiently deep convection (Figure 1) the initiation of strong downdraughts at the cloud edges play an important role. Apparently there are two ways in which organization occours. The first, which occurs in both strong and weak cumulus convection, results from the competition between adjacent cloud circulations in the developing stage of convection (first few hours). Latent heat plays a decisive role in determining which cloud circulations grow at the expense of others in horizontal direction and, if the inversion is permitted to be eroded, also in vertical direction. If the latter is the case, cumulus congestus clouds can form, with sharp downdraughts at the edges, which are responsible for the second organizing mechanism. The intense downdraughts act as a strong dynamical forcing (when hitting the ground, they enforce updraughts), thus favouring the formation of new clouds nearby. The fact that the environment of the cumulus clouds is relatively moist strengthens this effect.

The pattern to which this leads can best be seen in run 4 (Figure 1d), in which the forcing has been turned off after 2.5 hours. In the fourth hour of simulation new clouds continually develop around to older ones while the latter decay. In addition, in this two-dimensional model flow, the small scale motion mechanically feeds the larger scale circulation. Although this circulation is rather weak, it modifies the moisture field in such a way that the humidity in the cloud region remains sufficiently high for condensation. In this way the system is able to produce a considerable amount of kinetic energy.

The organization of the clouds can also be seen in the power spectrum of the cloud distribution, which we have computed every 15 minutes for runs 1 and 3. Figure 8 shows the result averaged over these two runs as a function of time. It can be seen that the larger scale circulation appears after about 2.5 hours. Before that time there is no dominant scale present between wave number 1 (60 km) and wave number 18 (3.3 km).

For weak cumulus convection (Figure 2) the cell circulation is (at least partly) directly fed by the release of latent heat in the upward branch and cooling by evaporation in the outer regions. Dynamical

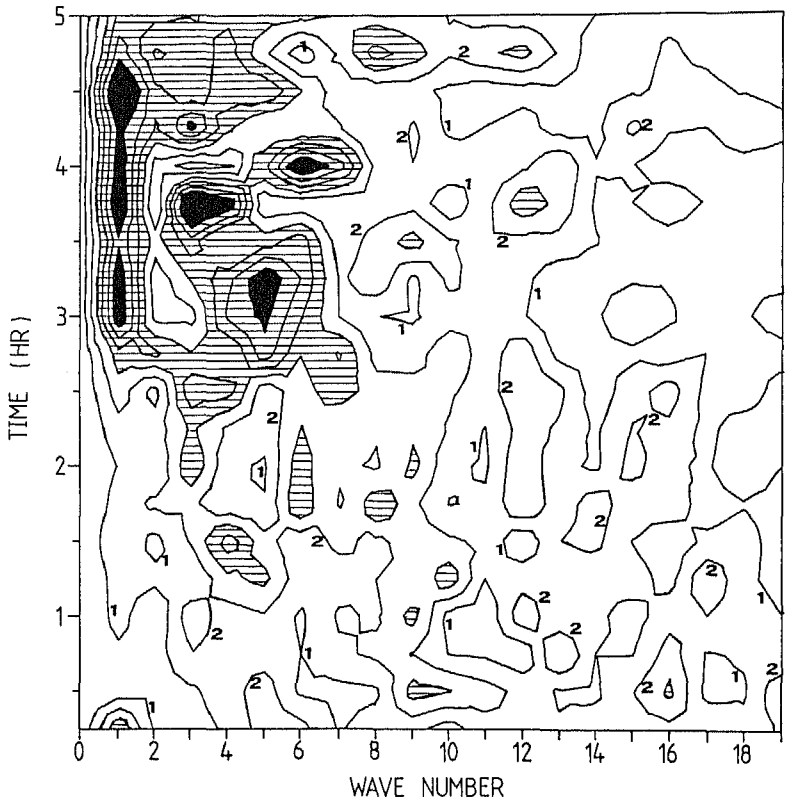

- Fig. 8 The power spectrum of the cloud distribution as a function of time, averaged over runs 1 and 3. The contour interval is 2.10^{-3} units of total variance. Regions between contour (3) and (6) are hatched. Regions above contour (6) are black.

- Bild 8 Das Varianz-Spektrum der Wolkenverteilung als Funktion der Zeit gemittelt über die Rechenläufe 1 und 3. Das Konturen-Intervall ist $2 \cdot 10^{-3}$ Einheiten der Gesamt-Varianz. Die Gebiete zwischen den Isolinien (3) und (6) sind schraffiert, die Gebiete oberhalb von (6) sind schwarz.

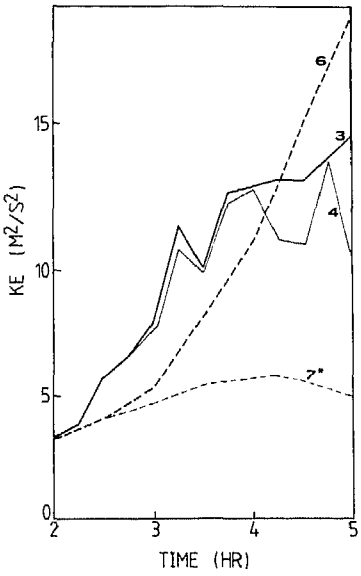

Fig. 9 Heavy lines show the kinetic energy for runs 3 (upper boundary at 4 km) and 6 (upper boundary at 2.2 km). The thin lines give the kinetic energy for the corresponding runs in which the heating was turned off after 2.5 h (runs 4 and 7*, see Table I).

Bild 9 Die dicken Linien zeigen die kinetische Energie für die Rechenläufe 3 (obere Grenze bei 4 km) und 6 (obere Grenze bei 2,2 km), die dünnen Linien für die Läufe 4 und 7*, bei denen die Heizung nach 2,5 h eingestellt wurde (siehe Tabelle I).

forcing on the small scale, which was very important in the case of strong convection, is virtually absent. This is illustrated in Figure 9. The heavy lines show the kinetic energy for run 3 (strong convection, solid) and run 6 (weak convection, dashed). The kinetic energy for the corresponding runs in which the forcing is stopped after 2.5 hours is indicated by the thin lines (runs 4 and 7*, see Table I). In the case of weak cumulus convection, the kinetic energy hardly increases after the heating has been turned off. In the case of strong cumulus convection, the kinetic energy increases substantially in spite of the absence of heating.

The reason why the small clouds in run 6 (Figure 2) drift away from the mother cloud with such great velocities (about 8 m/s at 4 h to about 15 m/s at 7 h (run 7)) is that they get caught in the intense outflow, just under the inversion, of the main cell circulation. In three dimensions this outflow would be less intense, because then the air would have the freedom to flow out radially.

In all experiments the model seems to hesitate whether it should produce one or two clumps of clouds. It is thus tempting to conclude that the system prefers a length scale of 15 to 20 km (or 30 km to 40 km from clump to clump). This immediately raises the question of whether our results can be linked to the roll and cellular cloud patterns that frequently occur in reality, especially in cases when cold air flows over a relatively warm ocean (see BRIMACOMBE, 1981, for fine examples). AGEE and DOWELL (1974), in diagnosing cellular convection, showed that a typical cell diameter is about 30 km. Inspection of satellite pictures reveals that the cloudy part of an open cell consists of many cumulus clouds (and not just a ring of steady cloud cover). The structure in a cross-section of an open cell, as inferred from satellite observation, is thus very similar to our results on strong convection. In view of this, we suggest that the moisture field plays a decisive role in the creation of roll and cellular convection. This casts some doubt on the similarity between classical Bénard-convection and cellular cloud patterns in the atmosphere (see also KRISHNAMURTI, 1975).

We realize that the model we use is two-dimensional and cannot produce cellular cloud patterns (which are really three-dimensional). Moreover, in two dimensions one cannot distinguish between open and closed cells. Adding to this the fact that in the model horizontal pressure variations were excluded, that the domain size imposes a length scale, and that precipitation was excluded (which makes the big clouds rather 'heavy' and therefore prone to collapse under their own weight), it is obvious that we cannot draw

firm conclusions. However, our experiments have revealed some interesting aspects of cloud organization and have posed some questions. In the future we will do more specific experiments with regard to the most interesting one: 'what determines the clump dimension?'.

Appendix

a. List of symbols

Scalars:

B	buoyancy
L	latent heat of condensation
R_a	gas constant for dry air
T	temperature
T_v	virtual temperature
c	weighted specific heat capacity of a mixture of air, water vapour and liquid water
c_p	specific heat of dry air at constant pressure
c_{pv}	specific heat of water vapour at constant pressure
c_w	specific heat of liquid water
e_s	saturation vapour pressure
g	acceleration due to gravity
p	pressure
r_l	mixing ratio of liquid water to dry air
r_s	saturation mixing ratio
r_v	mixing ratio of water vapour to dry air
t	time
u	horizontal component of wind
w	vertical component of wind
x	horizontal coordinate
z	vertical coordinate
ϵ	ratio of molecular weights of water vapour and dry air
η	horizontal (y–) component of vorticity
ρ	density
ν	coefficient of eddy diffusion of momentum, water substance or temperature
Ψ	stream function

Vectors:

$\mathbb{V}$	wind velocity
$\hat{k}$	vertical unit vector

b. Hydrodynamic equations

The basic hydrodynamic equations are based on the Boussinesq approximation, which holds for convection that is only a few kilometers in depth (SPIEGEL and VERONIS, 1960):

$$\frac{\partial \mathbb{V}}{\partial t} + \mathbb{V} \cdot \nabla \mathbb{V} = -\frac{1}{\rho} \nabla p' + B\hat{k} + \nu \nabla^2 \mathbb{V}, \tag{A1}$$

$$\nabla \cdot \mathbb{V} = 0, \tag{A2}$$

where the bouyancy force

$$B = \left(\frac{T_v'}{T_{v_m}} - r_l\right) g, \tag{A3}$$

and the virtual temperature T_v is defined as

$$T_v = \frac{1 + r_v/\epsilon}{1 + r_v} T. \tag{A4}$$

We have expressed any one of the state variables (f = T, ρ or p) in the form

$$f(x, z, t) = f_m + f_0(z) + f'(x, z, t),$$

where f_m is the (constant) space average of f; f_0 is the variation in f in the absence of motion; and f′ is the fluctuation resulting from motion.

It is convenient to use a streamfunction $\Psi(x, z)$ (so (A2) is directly satisfied):

$$u = -\frac{\partial \Psi}{\partial z} \quad \text{and} \quad w = \frac{\partial \Psi}{\partial x}. \tag{A5}$$

From (A1) and (A2) a vorticity equation can easily be derived. The y-component of this equation is

$$\frac{\partial \eta}{\partial t} = -u\frac{\partial \eta}{\partial x} - w\frac{\partial \eta}{\partial z} - \frac{\partial B}{\partial x} + \nu\left(\frac{\partial^2 \eta}{\partial x^2} + \frac{\partial^2 \eta}{\partial z^2}\right). \tag{A6}$$

where η is the y-component of the vorticity:

$$\eta = -\left(\frac{\partial w}{\partial x} - \frac{\partial u}{\partial z}\right) \quad \text{and} \quad \eta = -\left(\frac{\partial^2 \Psi}{\partial x^2} + \frac{\partial^2 \Psi}{\partial z^2}\right). \tag{A7}$$

Equation (A6) integrated in time by means of the Lax-Wendroff scheme (e.g. MESINGER and ARAKAWA, 1976). The last four terms on the righthand side of (A6) are computed using central differences in space. This scheme proved to be stable enough for the long runs we made with the model. In fact the timestep is determined by the truncation error in the Lagrangian part of the model (see below) rather than by the usual stability criteria. We used a time step of 10 s as a compromise between truncation error and computational efficiency. The Poisson equation (A7) is solved by succesive relaxation with boundary condition $\Psi \equiv 0$ on the boundary of the model domain.

With this scheme and the 4 by 60 km grid, a 5 hour real time simulation takes about 50 min CPU time on a CRAY–1 computer (including diagnostics).

c. Thermodynamics

The changes of T, r_v and r_l over a timestep are computed in a Lagrangian manner. This involves the following steps: (1) the determination of the upstream point from which air will arrive after a finite time step; (2) the determination of T, r_v and r_l at this point by bilinear interpolation; (3) a static readjustment of T, r_v and r_l, if necessary, so that neither relative humidity (RH) above 100 % nor liquid water at a RH below 100 % can occur; (4) a dynamical adjustment which accounts for condensation or evaporation while the "parcel" is advected to the grid point; (5) the adiabatic change of temperature by $-g/c$ K per m; (6) the computation of the rates of change of T, r_v and r_l by eddy diffusion which are given by $\nu\nabla^2 T'$, $\nu\nabla^2 r_v$ and $\nu\nabla^2 r_l$; (7) due to nonlinearities in most of the thermodynamical processes a repitition of (3) could be necessary. We eliminated the vertical diffusion of water vapour because it unrealistically erodes the sharp gradient in r_v at the inversion. This is especially important in run 6 where the inversion coincided with the upper boundary of the model domain.

The scheme is identical to that developed by MURRAY (1970) except for the formula we derived for the dynamical adjustment. This relation between dr_s/dt and w is derived using the following relations:

$$r_s = \frac{\epsilon e_s}{p - e_s}, \tag{A8}$$

$$\frac{de_s}{dt} = \frac{\epsilon L}{R_a T^2} e_s \frac{dT}{dt} \quad \text{(Clausius-Clapeyron equation)}, \tag{A9}$$

$$\frac{dT}{dt} - \frac{\omega}{\rho c} = -\frac{L}{c}\frac{dq_s}{dt} \quad \text{(first law of thermodynamics)}, \tag{A10}$$

where $\omega = dp/dt$ and q_s is the saturation specific humidity ($q_s = r_s/(1 + r_s)$). We also make use of the following relation between ω and w (HOLTON, 1979):

$$\omega = -\rho g w \tag{A11}$$

and of the equation of state for saturated air,

$$p = \rho \frac{R_a(r_s + \epsilon)}{\epsilon(r_s + 1)} T. \tag{A12}$$

If we differentiate (A8) to T and from the resulting equation we eliminate de_s/dt with (A9), dT/dt with (A10), ω with (A11) and ρ and e_s with (A12) and (A8), in this order, we then arrive at the relation

$$\frac{dr_s}{dt} = \frac{r_s((1 + r_s)cT - (\epsilon + r_s)L)gw}{R_a cT^2 + \frac{r_s L^2(\epsilon + r_s)}{(1 + r_s)^2}}. \tag{A13}$$

If $r_v = r_s$, $dr_s/dt = dr_v/dt = -dr_l/dt$.

References

AGEE, E. M. and K. E. DOWELL, 1974: Observational studies of mesoscale cellular convection. J. Appl. Meteor. 13, 46–54

BRIMACOMBE, C. A., 1981: Atlas of meteosat imagery. ESA Scientific & Technical Publications Branch.

HILL, G. E., 1974: Factors controlling the size and spacing of cumulus clouds as revealed by numerical experiments. J. Atmos. Sci. 31, 646–673.

HOLTON, J. R., 1979: An introduction to dynamic meteorology (second edition). Academic Press, New York, p. 72.

KRISHNAMURTI, R., 1975: On cellular cloud patterns. Part 3: Applicability of the mathematical and laboratory models. J. Atmos. Sci. 32, 1373–1383.

MESINGER, F. and A. ARAKAWA, 1976: Numerical methods used in atmospheric models. Garp Publication series no. 17.

MURRAY, F. W., 1970: Numerical models of a tropical cumulus cloud with bilateral and axial symmetry. Mon. Weather Rev. 98, 14–28.

PLANK, V. G., 1969: The size distribution of cumulus clouds in representative Florida populations. J. Appl. Meteor. 8, 46–67.

RANDALL, D. A. and G. J. HUFFMAN, 1980: A stochastic model of cumulus clumping. J. Atmos. Sci. 37, 2068–2078.

SPIEGEL, E. A. and G. VERONIS, 1960: On the Boussinesq approximation for a compressible fluid. The Astrophysical Journal 131, 442–447.

TAG, P. M., F. W. MURRAY and L. R. KOENIG, 1979: A comparison of several forms of eddy viscosity parameterization in a two dimensional cloud model. J. Appl. Meteor. 18, 1429–1441.

TELFORD, J.W. and J. WARNER, 1962: On the measurement from an aircraft of buoyancy and vertical air velocity in clouds. J. Atmos. Sci. 19, 415–423.

WARNER, J. and J. W. TELFORD, 1967: Convection below cloud base. J. Atmos. Sci, 24, 374–381.